REPORT DOCUMENTATION PAGE

Form Approved
OMB No. 0704-0188

1. REPORT DATE *(DD-MM-YYYY)*	2. REPORT TYPE	3. DATES COVERED *(From - To)*
	Final Technical Report	15 Apr 2003 – 14 Apr 2006

4. TITLE AND SUBTITLE
Experimental Micromechanics Study of Lamellar TiA1

5a. CONTRACT NUMBER

5b. GRANT NUMBER
F49620-03-1-0282

5c. PROGRAM ELEMENT NUMBER

6. AUTHOR(S)
Dr. Fu-Pen Chiang

5d. PROJECT NUMBER

5e. TASK NUMBER

5f. WORK UNIT NUMBER

7. PERFORMING ORGANIZATION NAME(S) AND ADDRESS(ES)
Research Foundation of State University of New York
Department of Mechanical Engineering
Stony Brook NY 11794-2300

8. PERFORMING ORGANIZATION REPORT NUMBER

9. SPONSORING/MONITORING AGENCY NAME(S) AND ADDRESS(ES)
Air Force Office of Scientific Research (AFOSR)
875 N. Arlington St., Rm. 3112
Arlington, VA 22203
Brett Conner/NA

10. SPONSOR/MONITOR'S ACRONYM(S)
AFOSR

11. SPONSORING/MONITORING AGENCY REPORT NUMBER
N/A

12. DISTRIBUTION AVAILABILITY STATEMENT
DISTRIBUTION A: Approved for public release. Distribution is unlimited.

AFRL-SR-AR-TR-07-0096

13. SUPPLEMENTARY NOTES

A unique micro-scale full field deformation measurement technique called electron speckle photography is exploited to investigate the deformation mechanism of lamellar TiAl. We find the size of the specimen used and the area of strain measurement affect the mechanical properties thus obtained. The strain distribution inside a grain is highly heterogeneous. The grain boundary is much stiffer than the interior of the grain. We also observe several interesting phenomena of the material when a crack is present. Crack speed tends to slow down when the crack approaches a grain boundary. Within a grain the slowest propagation speed is when the lamellar layers are perpendicular to the crack. Crack may jump across a grain boundary and its propagation direction may be predicted by the strain concentration congregated near the grain boundary. By mapping the deformation field surrounding the crack tip, we can evaluate the mode mixity from the speckle results at different stages of crack propagation.

15. SUBJECT TERMS

16. SECURITY CLASSIFICATION OF:			17. LIMITATION OF ABSTRACT	18. NUMBER OF PAGES	19a. NAME OF RESPONSIBLE PERSON
a. REPORT	b. ABSTRACT	c. THIS PAGE			19b. TELEPONE NUMBER *(Include area code)*
Unclassified	Unclassified	Unclassified	Unclassified	24	(703)

Final Report
AFOSR Grant# F49620-03-0282

Title	Experimental Micromechanics Study of Lamellar TiAl
Program Manager	Brett P. Conner, Capt (Ph.D.), USAF Program Manager, Metallic Materials Research AFOSR/NA 875 North Randolph Street Suite 325, Room 3112 Arlington, VA 22203-1768 (703) 696 8523 (DSN 426) (703) 696 8541 (FAX brett.conner@afosr.af.mil
Principal Investigator	Fu-pen Chiang, Ph.D. SUNY Distinguished Professor and Chair Department of Mechanical Engineering Stony Brook, NY 11794-2300 (631) 632-8311 (631) 632-8544 (FAX) Fu-pen.Chiang@stonybrook.edu
Date	February 15, 2007

Experimental Micromechanics Study of Lamellar TiAl

AFOSR GRANT #F49620-03-0282

Fu-pen Chiang

Department of Mechanical Engineering

State University of New York at Stony Brook

Abstract

A unique micro-scale full field deformation measurement technique called electron speckle photography is exploited to investigate the deformation mechanism of lamellar TiAl. We find the size of the specimen used and the area of strain measurement affect the mechanical properties thus obtained. The strain distribution inside a grain is highly heterogeneous. The grain boundary is much stiffer than the interior of the grain. We also observe several interesting phenomena of the material when a crack is present. Crack speed tends to slow down when the crack approaches a grain boundary. Within a grain the slowest propagation speed is when the lamellar layers are perpendicular to the crack. Crack may jump across a grain boundary and its propagation direction may be predicted by the strain concentration congregated near the grain boundary. By mapping the deformation field surrounding the crack tip, we can evaluate the mode mixity from the speckle results at different stages of crack propagation.

I. Research Objective

To Map the deformation of TiAl at micrometer scales under various loading conditions inside a scanning electron microscope to understand the mechanics and physics of the material.

II. Introduction

Titanium aluminide (TiAl) alloys based on lamellar TiAl are potentially important materials for future high performance jet engines. Among the advantages of lamellar TiAl are low density, oxidation resistance, high resistance to fracture and maintaining strength at high temperature. Depending on the concentration of Al and heat-treatment processes, TiAl alloys may assume different phases [1]. The microstructure of the material can be manipulated based on the heat-treatment process. Experiments done with different microstructures indicate that when compared with other microstructures fully-lamellar microstructures show more desirable properties such as higher fracture toughness and stable crack growth [2, 3, 4] .

The microstructure of lamellar TiAl consists of randomly oriented grains of two phases TiAl (γ) and Ti_3Al (α_2). Fig. 1 shows the grains with different orientations and platelets in one grain. Platelets inside in the grain are not ordered like γ/α_2 pairs. Typically the volume fraction of γ platelets are higher [5].

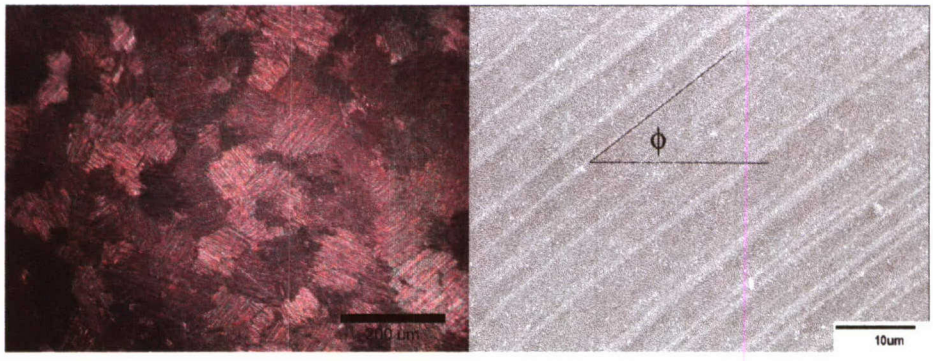

Figure 1. Optical & SEM Micrographs of Polycrystalline Lamellar TiAl.

There exists a fair amount of literature dealing with the failure mechanisms of TiAl [6-9] or fracture mechanics [10-16]. From the point of view of first-principles quantum mechanical studies or continuum mechanical models [17, 18] and atomistic simulations [19, 20].

In this paper we present some results of three sets of experiments in an effort to shade same light on the failure mechanism of TiAl from an experimental micromechanics point of view. The first set of experiments was designed to evaluate the size effect on the determination of mechanical properties. The information is of course crucial it one is to construct an analytical or numerical model to predict the mechanical response of this material under various loading conditions. The second set of experiments was design the mechanism of crack propagation in TiAl under Mode I loading using SEN (single edge notch) specimens. The third set of experiments was designed to investigate the propagation mechanism under mixed mode loading using cracked Brazilian disk specimens.

III. The Methodology of Electron Speckle Photography

Unique to our study is the employment of the electron speckle photography (ESP) technique [21]. The basic of ESP technique is described in the following: A micro or nano speckle pattern consisting of a random array of particles (either from commercial sources or by a physical vapor deposition process) is first created on the specimen surfaces, which is loaded in situ inside the chamber of a scanning electron microscope (SEM). This speckle pattern is recorded digitally and sequentially under incrementally applied load to the specimen. The resulting specklegrams are "compared" using a specially created software called CASI (Computer Aided Speckle Interferometry) [21, 22, 23].

Let $h_1(x, y)$ be the complex amplitudes of the light disturbance of a generic speckle subimage before deformation and $h_2(x, y)$ be the original speckle pattern with displacement components added, i.e.,

$$h_2(x,y) = h_1[x - u(x,y), y - v(x,y)] \qquad (1)$$

where u and v are the displacement components along the x and y directions, respectively, of the subimage "point". First a FFT is applied to both h_1 and h_2. Then, a numerical "interference" between the two speckle patterns is performed on the spectral domain as follows,

$$F(\omega_x,\omega_y)=\frac{H_1(\omega_x,\omega_y)H_2^{*}(\omega_x,\omega_y)}{\sqrt{\left|H_1(\omega_x,\omega_y)H_2(\omega_x,\omega_y)\right|}}=\sqrt{\left|H_1(\omega_x,\omega_y)H_2(\omega_x,\omega_y)\right|}\exp\{j[\phi_1(\omega_x,\omega_y)-\phi_2(\omega_x,\omega_y)]\} \tag{2}$$

where $\phi_1(\omega_x, \omega_y)$ and $\phi_2(\omega_x, \omega_y)$ are the phases of $H_1(\omega_x, \omega_y)$ and $H_2(\omega_x, \omega_y)$, respectively, and * denotes complex conjugate. Finally, a halo function is obtained by a second FFT, i.e.,

$$G(\xi,\eta)=\Im\{F(\omega_x,\omega_y)\}=\overline{G}(\xi-u,\eta-v) \tag{3}$$

which is an expanded impulse function located at (u, v) of the ξ and η plane. Thus, by detecting the crest of this impulse function, the displacement vector represented by the cluster of speckles within the subimage is uniquely determined. Strains are calculated using an appropriate strain-displacement relation. By recording the speckle image at incremental loads, strains of almost any finite magnitude can be obtained.

Thus, by searching for the peak of the delta function, the displacement vector representing the average displacement of all the speckles within the subimage. The distribution of the displacement vector can be used for strain calculation, depending upon the strain-displacement equation used. Since TiAl is a very brittle material, the following strain displacement relation were used:

$$\varepsilon_{xx}=\frac{\partial u}{\partial x},\ \varepsilon_{yy}=\frac{\partial v}{\partial y}\ \text{and}\ \varepsilon_{xy}=\frac{1}{2}\left(\frac{\partial u}{\partial y}+\frac{\partial v}{\partial x}\right) \tag{4}$$

This process of data analysis is employed in all the experiments performed.

IV. Size effect on Mechanical Properties of TiAl.

Average grain size of TiAl used in uniaxial tests is about 100μm. Fig.2 shows the dimensions of the TiAl specimen. In uniaxial test specimen the strain distribution is highly non-uniform.

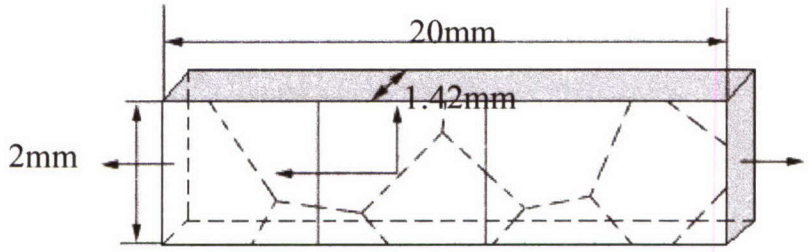

Figure 2. Dimension of TiAl specimen

An example is shown in Fig. 3 where the strain variation along a particular section is shown together with the entire deformation field in an area about 250μm x 250μm. It is seen that the strain at the boundary of two grains is about 7 times less than that of those in the interior of the grain.

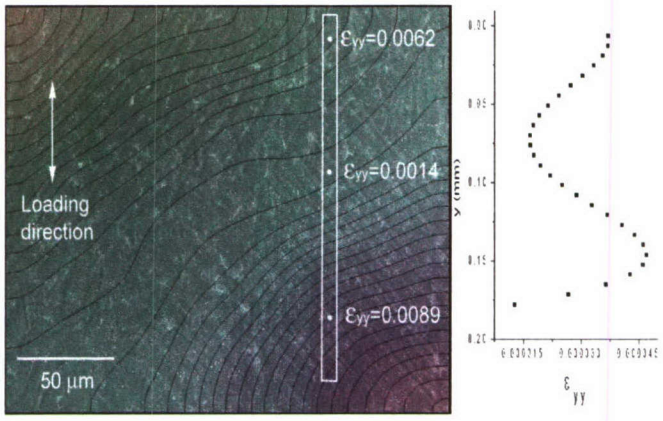

Figure 3. Strain variation along a vertical axis in a polycrystalline TiAl specimen under uniaxial tension

We selected a region of another specimen to observe its strain variation as a function of a monotonically increasing load. And we find the strain response under the same load history is a

function of the strain mapping area. If the strain mapping area is 2.85mm x 2.22mm, the stress-strain relation is fairly linear as one would expect for a homogenous material (see Fig. 4).

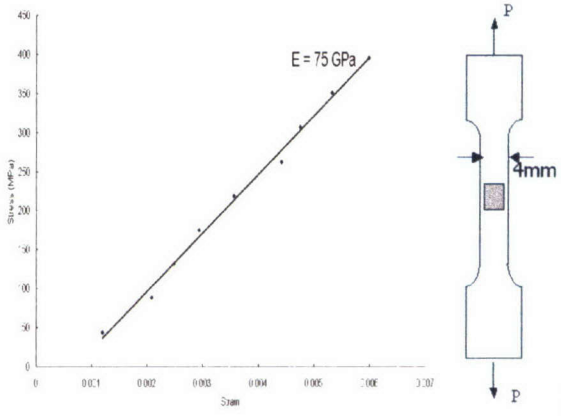

Figure 4. Global (averaged over 2.85mmx2.22mm) Stress-Strain Relationship of a γ-TiAl Specimen under Uniaxial Tension

However, if the strain measuring area is 0.23mm x 0.18mm, the ε-σ curve became highly nonlinear and the strain seems to zigzag as the load is monotonically increased at the early part of the deformation (see Fig. 5). When the strain area was further reduced to 7μm x 7μm, even more interesting phenomena were observed.

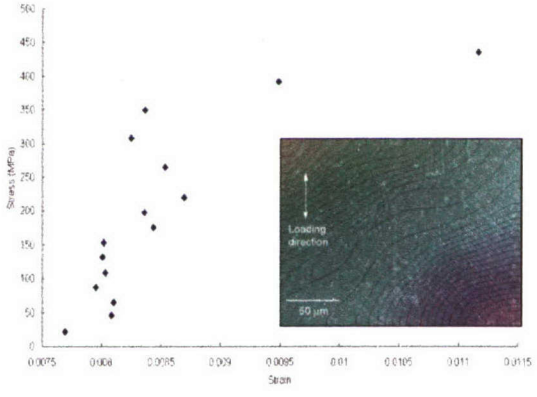

Figure 5. Macro (averaged over 0.23mmx0.18mm) Stress-Strain Relationship of a γ-TiAl Specimen under Uniaxial Tension

The magnitudes of the strain response of three points along a vertical section are depicted in Fig. 6. It is seen that the strain at the interior of the grain are some 4 times larger than that at the grain boundary.

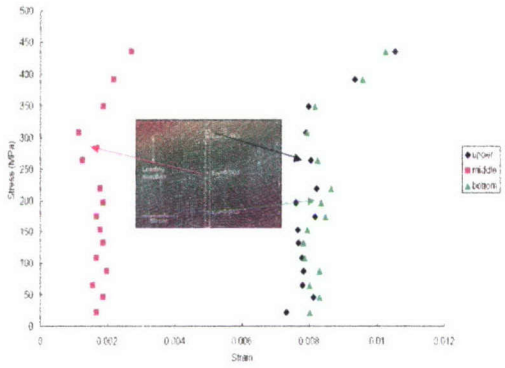

Figure 6. Micro (averaged over 7μmx7μm) Stress-Strain Relationships of a γ-TiAl Specimen under Uniaxial Tension

And the strain difference between the two points remained fairly constant as the load was increased. We also note a zigzagging nature of the earlier part of the stress strain curve. In all three cases the strains at the later stage of the deformation increase almost linearly with respect to the load.

V. Crack Propagation under Mode I Loading

Geometry of the specimens is shown in Fig.7. The specimens were loaded by tension inside the chamber of Hitachi S2460N scanning electron microscope. All tested specimens had a natural initial crack initiated by fatigue. Surfaces of the specimens were coated with random particles made of copper with size ranging from 0.5 μm to 5 μm. The surface of the specimen together with the speckle pattern was recorded digitally at various incremental loads. The loading was displacement controlled via two sets of screws at a rate of 4 μm/sec. The loading was stopped whenever we observed a sudden drop in load indicating that the crack has extended. And a SEM

picture was recorded. The process takes about 1 minute. Then loading is resumed until fracture ensues.

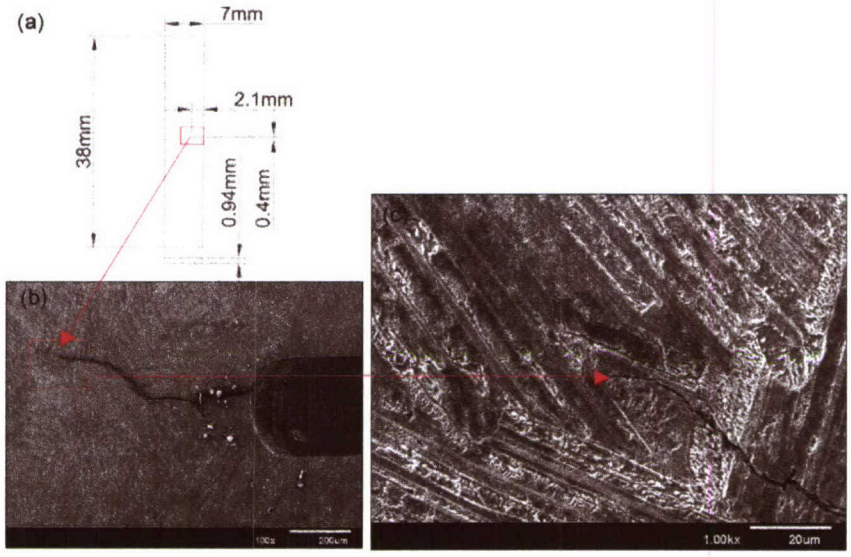

Figure 7. (a) Geometry of SEN Specimen,(b) Initial Crack Generated by Fatigue, (c) Initial Crack with Larger Magnification

As shown in Fig. 7 the fatigue initiated crack from the notch has just propagated through a grain with orientation almost perpendicular to crack path. And it is arrested at the junction of many grains concentrating together (see the enlarged view).

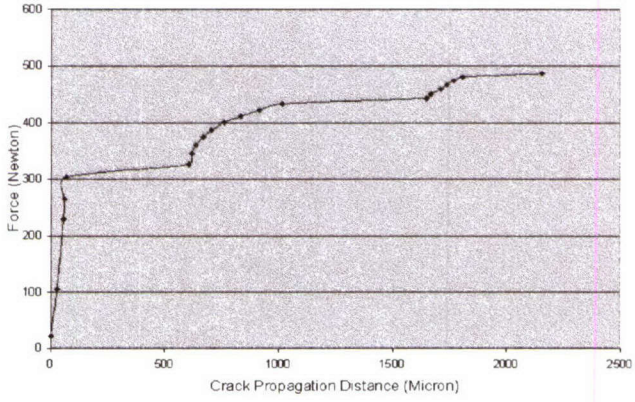

Figure 8. Load-Extension History of a Crack in a Simple Tension Specimen with a Single Edge Notch

The picture shown in Fig.7 indicates that the initial fatigue crack was arrested when it reached the junction of a cluster of grains. And the crack-extension curve in Fig. 8 implies that there is considerable resistance for the crack advance. Indeed the picture in Fig. 9 at a load of 5 lbs.

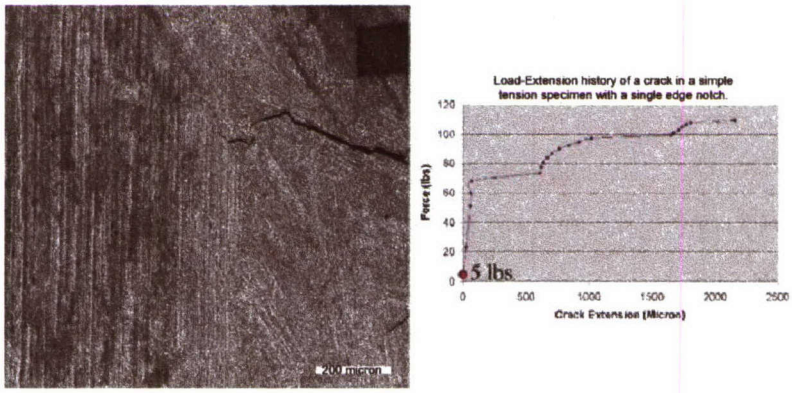

Figure 9. Crack Extension as a Function of Load

While the initial crack did not extend much, for this load another crack had started to appear below the main crack. As the load was further increased, both the main and the secondary crack extended simultaneously but at different rates, until the load reached 68.4 lbs. As shown in Fig. 10, an additional load to 73.5 lbs. caused the crack to jump across a grain boundary. The crack tip again was arrested in the middle of a cluster of grains.

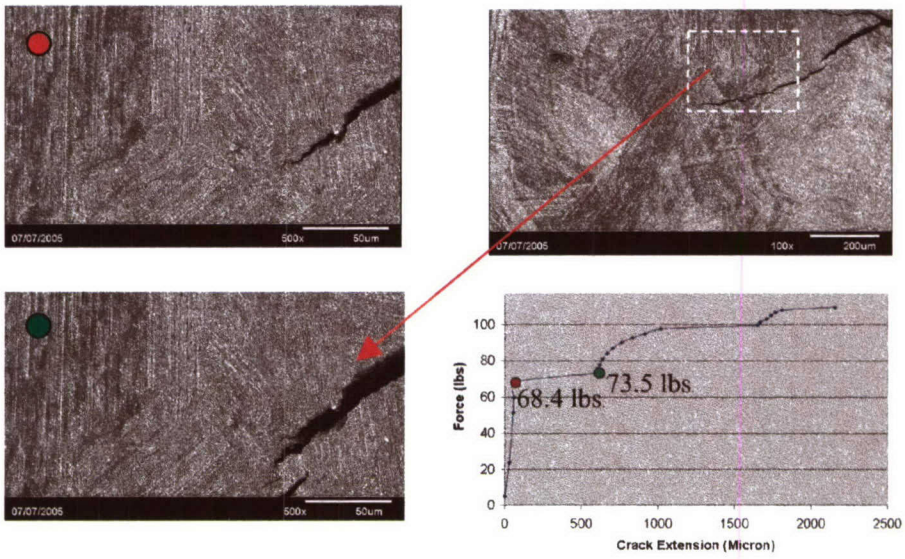

Figure 10. The Secondary Crack Jumped across Grain Boundary

Considerable resistance to further crack extension was again evident when the load was increased from 73.5 lbs. to 97.5 lbs. as shown in Fig.11.

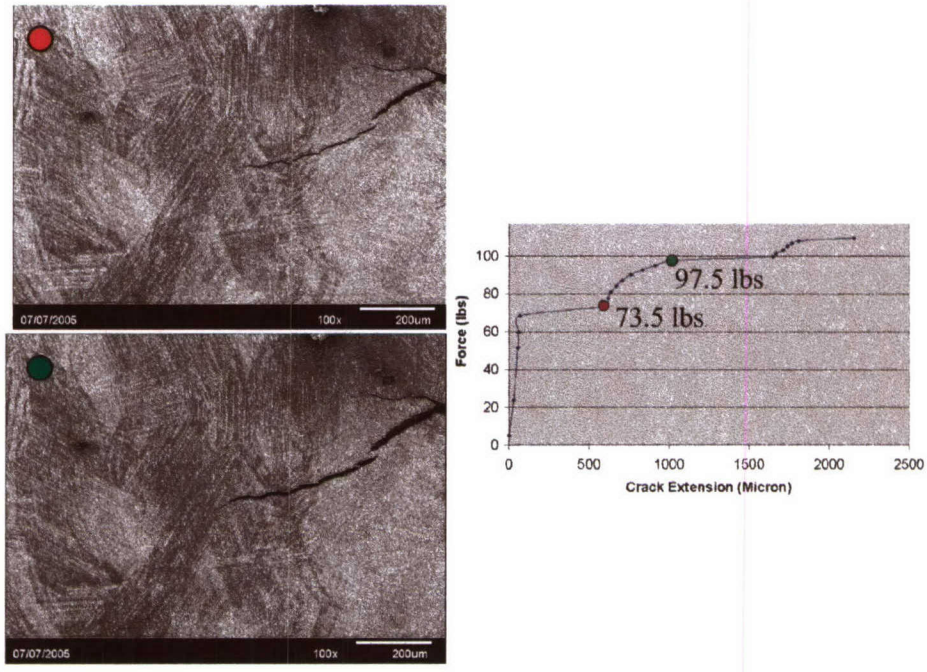

Figure 11. Slow Crack Growth Period between P = 73.5 lbs. and P = 97.5 lbs

Another slow growth period as shown in Fig.12 where it is seen that between the loads 101.3 lbs. and 108.1 lbs. the crack was laboring thorough a cluster of grains with various orientations. Further increase of the load resulted in unstable crack propagation which was not observable in SEM.

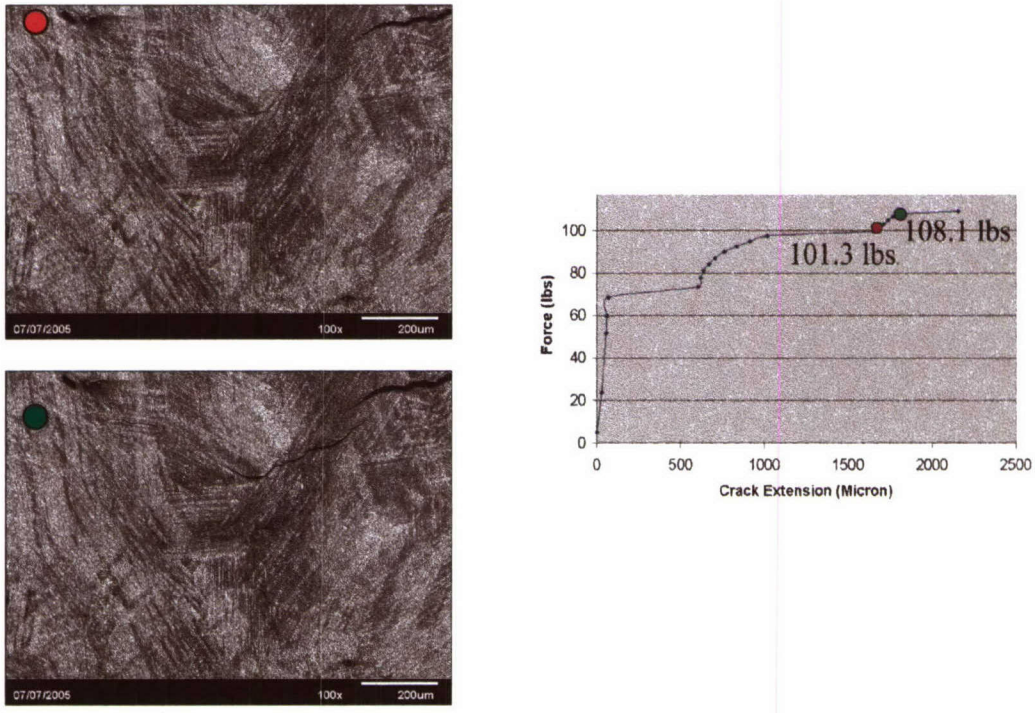

Figure 12. Slow Crack Growth Period between P = 101.3 lbs. and P = 108.1 lbs.

VI. Crack Propagation Under Mixed Mode Loading

Cracked Brazilian Disk (CBD) specimens were manufactured from the lamellar TiAl. Geometry of the specimens is shown in Fig.13

Specimen	A*	B**	C**	D**	E**	F**	G**	H**	K**	L**
D (mm)	9	7	3.2	3.2	4	4	4	7	9	9
A (mm)	1.45	1.45	1.45	1.45	1.45	1.45	1.45	1.45	1.45	1.45
2a/D	0.17	0.17	0.2	0.2	0.2	0.2	0.2	0.17	0.2	0.17
β	143 °	149°	0°	32°	32°	57°	7°	34°	25°	20°

* Specimens tested with Instron Machine
** Specimen tested with SEM

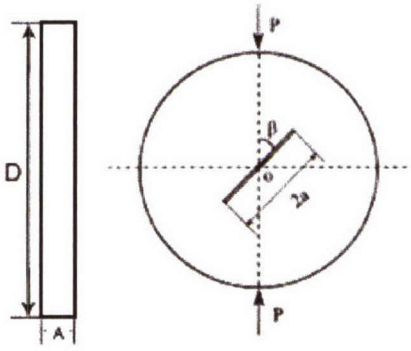

Figure 13. Geometry of the Cracked Brazilian Disc Test Specimen

As shown in Fig. 14, specimen A was loaded to 430 lbs. Further loading led to failure without obtaining any additional information. Examination of the v-field displacement contour indicates the strain concentration at the tips of the central slot.

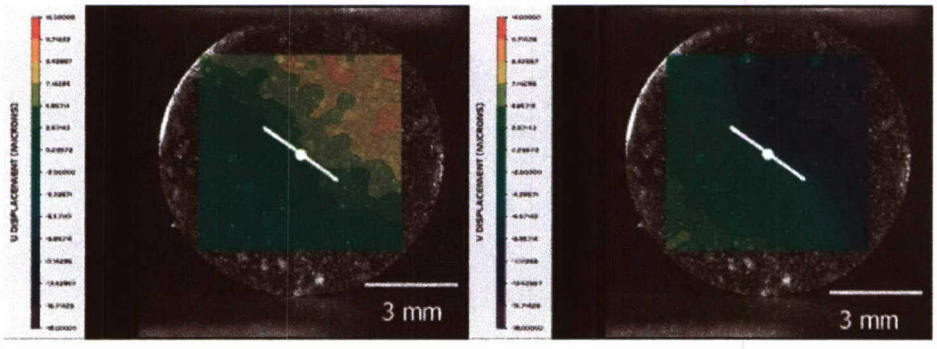

Figure 14. Displacement Fields of a 9 mm Brazilian Disk Under Compression Prior to Crack Initiation.

In order to reveal more information at the crack tip, several CBD specimens were tested inside SEM and viewed at different magnifications. To control the deformation mode we used the results given in Fett. *et al* [24]. Specimen B (β =149°) was tested in mixed mode. Fig. 15 shows the displacement field under a load of 287 lbs. Examination of the v-field displacement contour reveals that the highest fringe density (thus the highest ε_{yy}) occurs at the point where the straight line edge of the slot meets the curved surface.

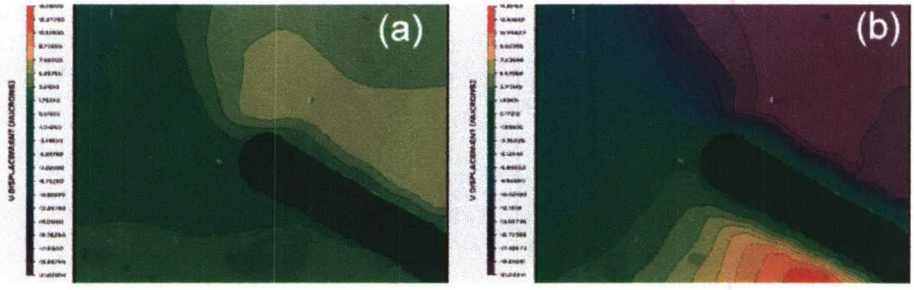

Figure 15. Displacement Fields of Specimen B Prior to Crack Initiation. (a) U-field (b) V-field

An additional loading to 290 lbs result the simultaneous appearance of two cracks at the ends of the slot and load dropped to 287 lb. The locations are indeed at the points where the straight and curved edges meet as shown in Fig.16.

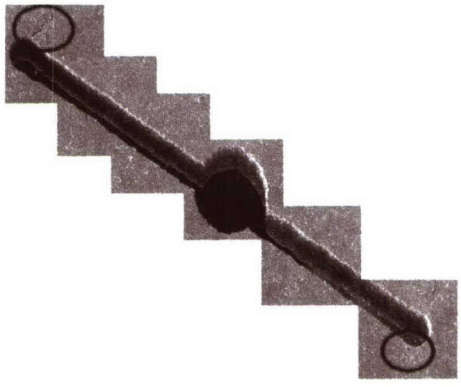

Figure 16. Two Cracks Appear at the Ends of the Central Slot of the 7mm Brazilian Disc.

Further loading of P = 287 lb to P = 291.4 lb did not advance the crack much (only a few microns). This is the region where the crack was arrested in the triple junction of grains. The displacement contours of an incremental load of P = 282.3lb to P = 288.7 lb are shown in Fig. 17. Also shown in the figure is the crack tip position relative to the grains. Additional load caused the crack to propagate unstably and led to dynamic fracture of the specimen.

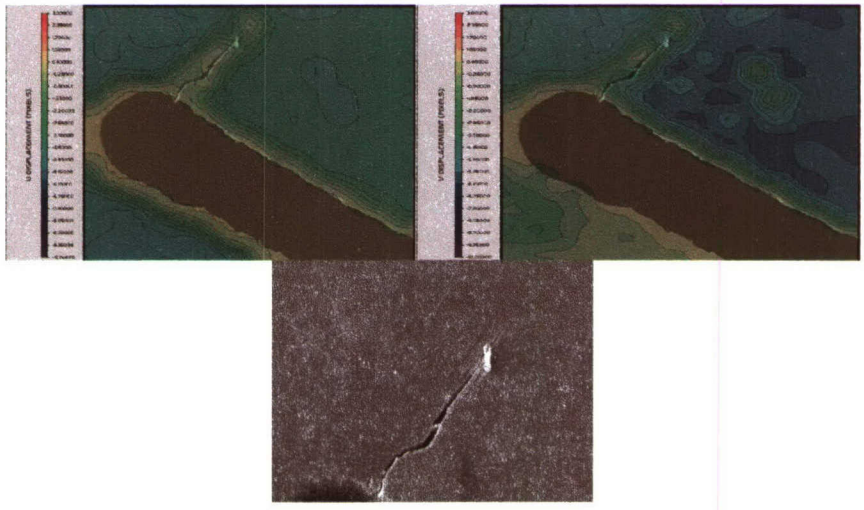

Figure 17. Crack Tip Deformation Fields and Location

Specimen C was tested in mode I (β=0°). Fig. 18 (a) and Fig. 18 (b) depicts the deformation pattern prior to crack initiation. Fig. 18 (c) shows a crack initiated at the bottom tip of the central crack at P=190 lb. With further loading the crack started to propagate. At the load P= 263 lb crack tip approached to grain boundary and two cracks on bottom and above of the central crack initiated which was parallel to grain orientation. When loading continued the first crack entered a blunting process, with larger crack opening displacement as the load increased.

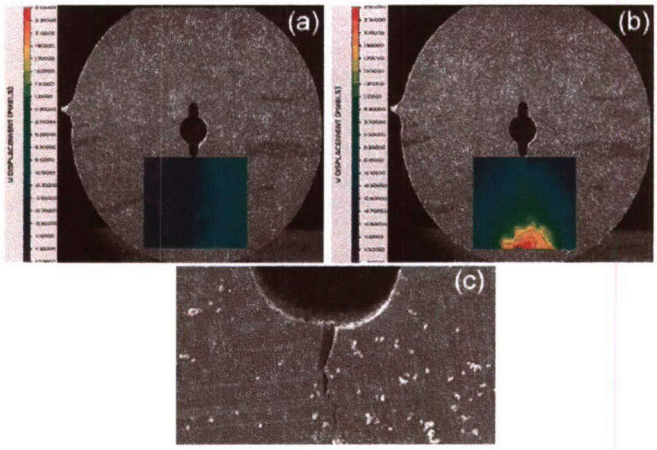

Figure 18. Displacement Fields of Specimen C Prior to Crack Initiation. (a) U-field (b) V-field. (c) Crack after Initiation.

As illustrated in Fig. 19 as second crack on the bottom started to link itself with the first crack. After the two cracks met in the same grain and they linked themselves with a ligament. Further loading to P=344 lb broke the disk into two pieces

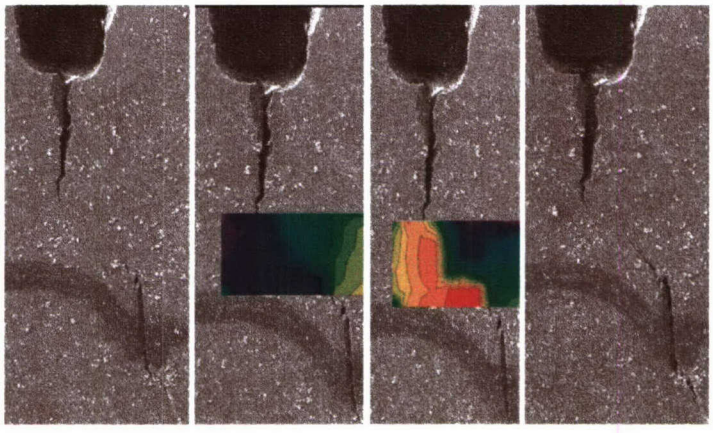

Figure 19. Linkage between Two Cracks via Mode II.

Specimen D was tested with β=32o as shown in Fig.20. Cracks above and below the central crack were initiated at P=166 lb and P=183 lb respectively. The upper semi crack approached to a grain boundary whose orientation was nearly perpendicular to crack. The crack was arrested in that region and blunting process started. With further loading another crack initiated near the upper crack in the same direction with the grain. Lower semi crack did not met to a grain with normal orientation. Thus it continued to propagate as further loading was applied and the failure occurred.

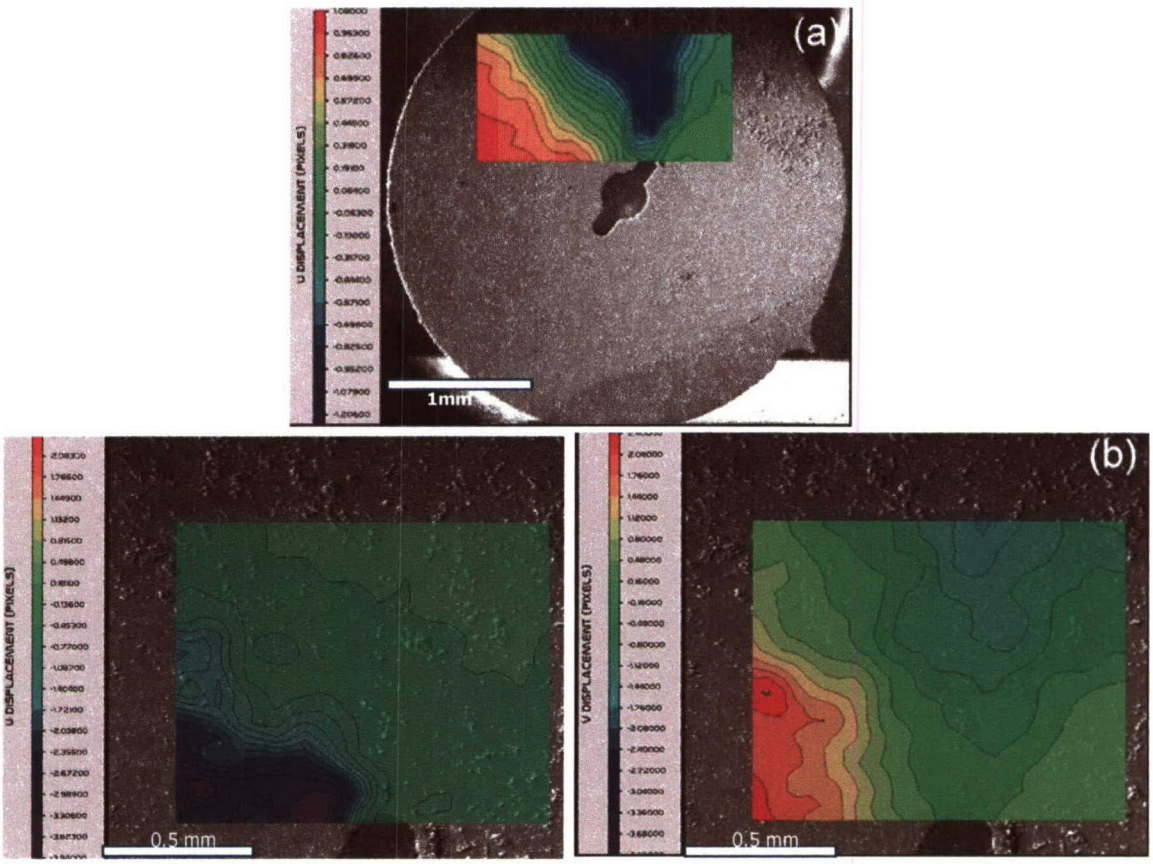

Figure 20. Displacement and strain field in specimen D.

During the tests we observed microcracks in front of the main crack tips. These microcracks were initiated with the orientation almost parallel to the loading direction and they propagated through the grain by extending the crack length in both directions.

VII. Discussion and Conclusions

In the early stage of uniaxial tests, we believe the non linear response is largely due to the re-arranging of the grains as the load is applied. Once the rearrangement is complete, the specimen will deform uniformly as the load further increases. For a given uniaxial tension specimen, the strain at the grain boundary can be seven times smaller than the interior of the grain. Also the experimental results demonstrate exclusively that grain boundaries act as crack retarders. Whenever a crack enters the junction of a cluster of grains, it slows down and seeks the path of least resistance; it tends not to propagate along the direction perpendicular to the lamellar layers. When the crack tip reaches the grain boundary, the direction of its further extension can be predicted by the strain field surrounding the crack tip region. Fig. 21 shows such an example. The shear strain field obtained by electron speckle photography technique indicates strain concentration appearing only on one side of the crack demonstrating that the strain free side is moving as a rigid body.

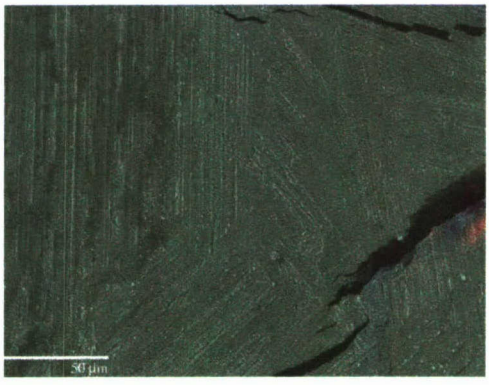

Figure 21. Shear Strain Field Prior to the Crack Jump across Grain Boundary.

The shear strain extents into a region where is no observable crack. And indeed it was the direction of crack propagation after the crack had jumped across the grain boundary. Another example can be given in Fig. 22. It shows the displacement and strain fields surrounding the upper edge of the notch in specimen C prior to crack initiation. Strain field indicates the area of high strain concentration. Further loading resulted in new mode I crack initiated at a distance away from the main crack in grain with orientation similar to the loading direction. Within the area indicated by of high strain concentration.

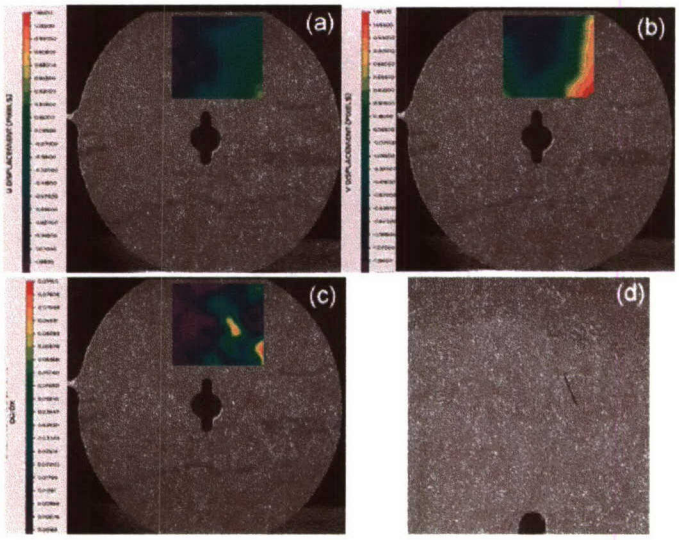

Figure22. Displacement Fields of Specimen C Prior to Crack Initiation. (a) U-field (b) V-Field.(c) ε_{xx} Strain Field.(d) Crack Initiated in the Site Indicated by Strain Field.

During the uniaxial tension test, microcracks that perpendicular to the grain orientation initiated but they did not propagate. In the case of Fig. 23, crack tends to change its orientation along the lamellar direction. Microcracks that parallel to the lamellar orientation were created in front of the main crack. At same time, a new crack which is perpendicular to the grain and the loading direction (arrow shown in Fig.23) is initiated. Then main crack was then connected with this new crack. In Fig.23 strain field ε_{xy} shows a clear shear band between the new and the main crack, in

this case indeed shear band plays an important role in the propagation mode resulting in the sliding of layers against each other and thus linking the main crack with the new crack. Even if there is a shear band, the magnitude of ε_{yy} seems to indicate that the crack faces would open as well.

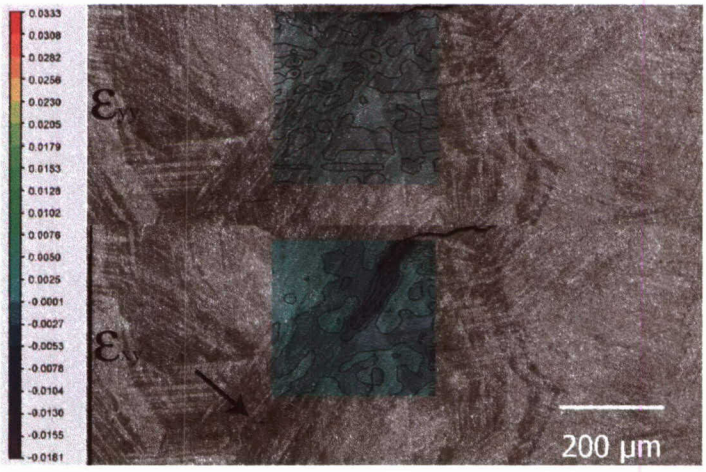

Figure 23. Strain Field Surrounding the Crack Tip between P= 90 lbs. and P= 100 lbs.

In case of Brazilian tests we also observed microcracks in front of the crack tip as depicted in Fig. 19 and Fig. 21. Different from uniaxial tests, these microcracks initiated in the same direction with grains (and also loading direction) and again main crack connected itself with these microcracks with shear band as shown in Fig. 19. It's worth to note that in uniaxial tests the microcracks in front of the main crack did not propagate after initiation, but in compression tests the microcracks initiated in the same direction with the grains and they propagated in both directions through the grain.

It could be depicted that crack propagation of lamellar TiAl is always in a mixed mode (I + II) unless the crack is perpendicular to the lamellar orientation. When the crack reaches a grain boundary normal to the crack, it blunts first and then penetrates the grain with a zigzagging path with a deformation where mode I is dominant. Thus crack assumes different mode mixity as it

meanders through different grains with different lamellar orientations. However at the end of the journey it always resorts to mode I propagation to failure. Fig 23 shows various examples.

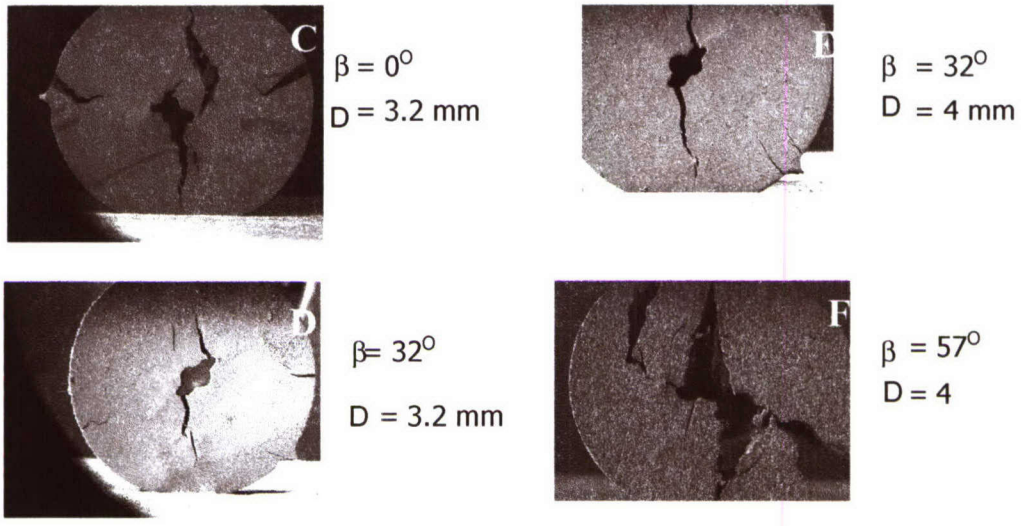

Figure24. Mode I Failure is the Dominant Failure Mode Irrespective of the Initial Slot Orientation.

Here we propose a technique that can evaluate the mode mixity from two representative displacement vectors on either side of the crack as illustrated in Fig. 24

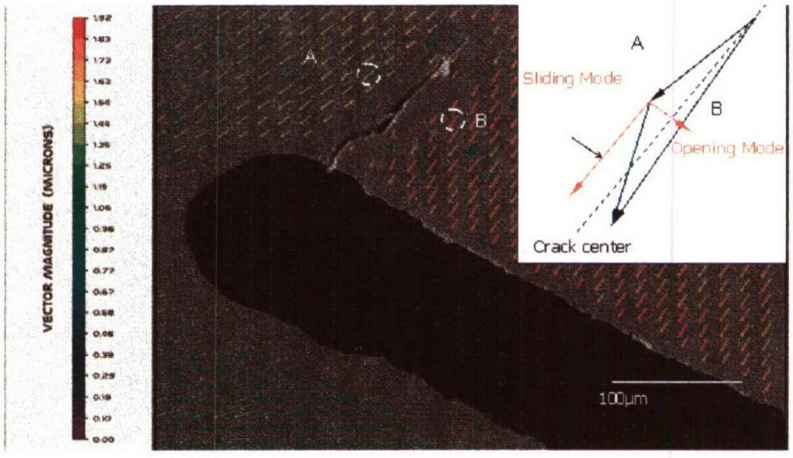

Figure24. Evaluation of Mode Mixity on CBD Specimen

It can be concluded that electron speckle technique is an effective tool to study crack propagation characteristics. In TiAl the grain boundary retards the crack advance by providing large amount of resistance. The weakest path of the $\gamma - \alpha_2$ lamellar TiAl is the interface of the $\gamma - \alpha_2$ layers. When a crack runs into the junction of a cluster of grains with different orientation the crack seeks the $\gamma - \alpha_2$ interface which changes its direction from place to place. This act tends to retard the crack propagation. This phenomenon may explain why smaller grain TiAl compounds tend to have high fracture toughness. Smaller grains have many more grain boundaries for the crack to cross.

References:

1. F. Appel, R Wagner, *Materials Science and Engineering*, *R*22 , p.187-268. (1998)
2. D.M. Dimiduk, Y. W Kim, R. Wagner, M. Yamaguchi (Eds.), Gamma Titanium Aluminides, TMS, Warrendale, PA, p.3. (1995)
3. Y. W. Kim, *JOM* 46, p.30. (1994)
4. Y. W. Kim, *Mat. Sci. Eng.*, *A*192/193, p.519. (1995)
5. *of Fracture* 105, p.321-342. (2000)
6. G. Hug, A. Louseau, P.Veyssiére, *Phil. Mag. A*57, p. 499. (1988)
7. B.F. Greenberg, Phys. *Status Solidi B*55, p.59. (1973)
8. M. Yamaguchi, Y. Umagoshi, *Prog. Mater. Sci.* 34, p.1. (1990)
9. K.J. Hemker, B. Viguer, M.J. Mills, *Mat. Sci. Eng. A*164, p.391. (1993)
10. K.S. Chan, Y. W. Kim, *Metall. Trans.* 23A, p.1663. (1992)
11. K.S. Chan, *Metall. Trans.* 24, p.569. (1993)
12. K.S. Chan, Y. W. Kim, *Metall. Trans.* 24A, p.113. (1993)
13. K.S. Chan, Y. W. Kim, *Acta Metal. Mater.* 43-2, p.439-451. (1995)
14. K.S. Chan, Y. W. Kim, *Metall. and Mat. Trans.* 25A, p.1217. (1994)

15. K.S. Chan, Donald S. Shih, *Metall. and Mat. Trans.* 28A, p.79. (1997)

16. K.S. Chan, Jessica Onstott, Sharvan Kumar, *Metall. and Mat. Trans.* 31A, p.71. (2000)

17. W. Wunderlich, Th. Kremser, G. Frommeyer, *Acta Metall. Mater.* 41, p.1791. (1993)

18. C.L. Fu, M.H. Yoo, *J Mater Res*.4, p.50. (1989)

19. C. Woodward, J.M. Mclaren, S.I. Rao, *J mater. Res.* 7, p.1735. (1992)

20. Z.C. Li, S.H. Whang, Mat. Sci. Eng., A152, p.18. (1992)

21. Chiang FP., *Solid Mechanics Archives*, 30, p.1. (1978)

22. Asundi, A. and Chiang F.P., *Optical Engineering* 24(4), p. 570. (1982)

23. Chiang FP., *Optical Engineering*, vol. 42(5), p.1288., (2003)

24. Fett T. *Eng. Fract Mech*, 68, p.1119–36. 2001

Personnel Supported

Kai Wang Graduate Student, Stony Brook University, Stony Brook

Dan Hong Graduate Student, Stony Brook University, Stony Brook

Yi Ding Graduate Student, Stony Brook University, Stony Brook

Gunes Uzer Graduate Student, Stony Brook University, Stony Brook

Sheng Chang PhD., Stony Brook University, Stony Brook

F.P. Chiang SUNY Distinguished Professor, Stony Brook University, Stony Brook

Publications

"Micro/Nanomechanics Mapping of Deformation Pattern of Lamellar of TiAl", F.P. Chiang, Keynote Paper, Proceedings of ICCESS '04, Madeira, Portugal, July 25~29,2004.

"A Micromechanics Study of α-TiAl under Uniaxial Tension", F.P.Chiang, S. Chang, and K. Wang, Proceedings of 2004 TMS Annual Conference _Symposium on Materials by Design: Atom to Application, Charlotte, NC, March 14~18, 2004.

"A Micromechanics Study of Lamellar TiAl", F.P.Chiang, S. Chang, K. Wang, and Andrew H. Rosenberger, Proceedings of the 2005 SEM Annual Conference & Exposition, Portland, OR USA, June 7~9, 2005

"Brazilian Tests in Lamellar TiAl", F.P. Chiang, Y. Ding, A.Ho, A.H. Rosenberger, G. Uzer, Proceedings of the 2006 SEM Annual Conference & Exposition, St. Louis, Missouri USA June 4~7, 2006

"Crack Propagation in Lamellar TiAl Under Mode I Loading", F.P. Chiang, Y. Ding, A.Ho, A.H. Rosenberger, G. Uzer, Proceedings of the 2006 SEM Annual Conference & Exposition, St. Louis, Missouri USA June 4~7, 2006

"Crack Tip Behavior in TiAl When Approaching Grain Boundary", F.P. Chiang, Y. Ding, A.Ho, G. Uzer, 16th European Conference of Fracture, Failure Analysis of Nano and Engineering Materials and Structrures, Alexandroupolis, Greece, July 3~7, 2006

"Advances in experimental mechanics : From Photoelasticity to Nanospeckle Techniques.", F.P. Chiang, Keynote Lecture, U.S. National Congress of Theoretical and Applied Mechanics, Boulder, CO, June 20~30, 2006

"Mixed mode Brazilian tests of lamellar TiAl", G. Uzer, F.P. Chiang, ICEM13 International Conference on Experimental Mechanics, July 1-6, Alexandroupolis, Greece, 2007

"Experimental Micromechanics Study of Lamellar TiAl", Fu-pen Chiang, Gunes Uzer, Andrew H. Rosenberger., 2007 TMS Annual Meeting, February 25 - March 1, Orlando, FL, 2007

"Crack Propagation in Lamellar TiAl Under Cyclic Loading", F.P. Chiang, Y. Ding, A.Ho, A.H. Rosenberger, G. Uzer, Proceedings of the 2007 SEM Annual Conference & Exposition, Springfield, Massachusetts USA June 3~6, 2007